Hindawi Publishing Corporation
International Journal of Oceanography
Volume 2014, Article ID 384618, 13 pages
http://dx.doi.org/10.1155/2014/384618

Research Article

Bio-Optical Characteristics of the Northern Gulf of California during June 2008

Martha Bastidas-Salamanca,[1] Adriana Gonzalez-Silvera,[2] Roberto Millán-Núñez,[2] Eduardo Santamaria-del-Angel,[2] and Robert Frouin[3]

[1] *Instituto de Investigaciones Marinas y Costeras, INVEMAR, Santa Marta, Colombia*
[2] *Facultad de Ciencias Marinas, Universidad Autónoma de Baja California, BC. Carr. Tijuana-Ensenada Km 103, 22800 Ensenada, BC, Mexico*
[3] *Scripps Institution of Oceanography, UC, San Diego, CA 92037, USA*

Correspondence should be addressed to Adriana Gonzalez-Silvera; adriana.gonzalez@uabc.edu.mx

Received 30 June 2014; Accepted 13 October 2014; Published 7 December 2014

Academic Editor: Heinrich Hühnerfuss

Bio-optical variables in the Northern Gulf of California were analyzed using *in situ* and satellite data obtained during a cruise in June 2008. The study area was divided into three bio-optical regions: Upper Gulf (UG), Northern Gulf (NG), and Great Isles (GI). Each region was characterized according to phytoplankton pigment concentration, phytoplankton and nonpigmented material spectral absorption coefficients, and spectral reflectance. Observed patterns were an indication of the shift in bio-optical conditions from north to south going from turbid and eutrophic waters to mesotrophic ones. Although there was a good agreement between satellite and *in situ* Chl*a* (RMSE ±33%), an overestimation of *in situ* Chl*a* was observed. This was partly explained by the presence of nonalgal particles, as well as the influence of desert and continental aerosols, which is generally overcorrected in the standard processing. The UG and NG could be considered as Case 2 waters, but they did exhibit different bio-optical characteristics. This implies that both biological and optical properties should be invoked to better understand water reflectance variability in the study region and its implications for the remote sensing of Chl*a* and biogeochemical processes.

1. Introduction

Observing the optical properties of the marine environment is crucial for the evaluation of satellite ocean color products and the development of spectral deconvolution techniques. Coastal zones are of particular interest, since they are influenced by mineral sediments, brought by rivers or stirred up from the bottom, as well as by colored dissolved organic matter of terrestrial origin (CDOM). In these zones, however, the algorithms (of the blue-to-green ratio type), developed for open ocean waters, generally fail, with the result of strongly overestimated chlorophyll-*a* concentration (Chl*a*) [1].

The Gulf of California is a subtropical semienclosed sea characterized by a cyclonic circulation in summer and an anticyclonic circulation in winter and by a seasonally reversible upwelling system with moderate upwelling along the west coast during summer and intense upwelling along the east coast during winter [2, 3]. In the northern part of the Gulf, that is, from the Colorado River Delta to 28°N (Figure 1(a)), these characteristics and also the bathymetry result in an eddy in the center of the basin and a coastal current on the mainland shelf. Direct observations show that the central eddy is ~150 m deep, cyclonic from June to September, and anticyclonic from November to April [4, 5]. Satellite observations have confirmed the cyclonic pattern during summer, but at the same time they have revealed a more complex circulation pattern with numerous plumes and eddies (some anticyclonic), traveling from coast to coast, enhancing the exchange of suspended material [6].

The Northern Gulf is mostly less than 200 m deep and tidal mixing is very important [7], especially around the sills of the midriff archipelago region (Great Isles, GI) and in

the shallow Upper Gulf (UG, north of 34°45′). The GI region and the sills are an area of continuous upward pumping of nutrients by tidal mixing [8, 9], while in the UG region tidal mixing has the same effect. These complex circulation patterns support very high primary production rates [8] and a high-diversity, high abundance fish fauna of commercial and ecological importance [10–12].

In the UG region tidal mixing is also responsible for the resuspension of inorganic material generating a zone of high turbidity [11], which can eventually be observed in true-color imagery of the area. For this reason these waters were classified as Case 2 while those to the south were classified as Case 1 waters [13]. However, the complex circulation patterns mentioned above may lead to a high spatial variability of such properties. In addition, the area studied by Pegau et al. [13] was located mostly to the south of the GI region and few stations covered the northern area.

In this context, the hypothesis is that there should be at least two distinct bio-optical regimes in the Northern Gulf of California that respond to the strong oceanographic heterogeneity of this zone. Based on the measurement of some surface bio-optical variables carried out in June 2008, the present study aims to (i) identify different bio-optical regions; (ii) evaluate the differences in spectral reflectance and spectral particulate absorption among identified bio-optical regions; (iii) evaluate the role of different phytoplankton communities among regions; and (iv) quantify the influence of these differences on the remote sensing of Chl*a*.

2. Methodology

2.1. Sampling Procedure. During June 2 to 17, 2008, 48 stations were made in the Northern Gulf of California, from 28° to 32°N and 112 to 115°W (Figure 1(a)). Water transparency was measured using Secchi disk from which we calculated the attenuation coefficient (Kd) and the first optical depth (1OD) [14]. Surface water samples (~0.40 m depth) were taken using Niskin bottles to measure phytoplankton pigments concentration and light absorption coefficient by particulate material.

In some stations, sampled between 10 a.m. and 3 p.m. and with clear sky conditions, marine reflectance ($R(\lambda)$) was measured using a SIMBADA radiometer, an improved version of the SIMBAD radiometer [15] that measures in spectral bands centered at wavelengths of 350, 380, 412, 443, 490, 510, 560, 620, 670, 750, and 870 nm [16]. The instrument was calibrated in the laboratory using an integrating sphere and in the field using a Spectralon plaque. Procedures described in Bécu [16] were applied to process the data into marine reflectance.

For pigment analysis, one to two liters (depending on station location) of seawater was filtered through 25 mm diameter Whatman GF/F filters with positive pressure. Filters were wrapped in aluminum foil and stored in liquid nitrogen until laboratory analysis. One or two liters of seawater was also filtered through Whatman GF/F filters for measurement of particulate light absorption. Filters were placed in Histoprep tissue caps and stored in liquid nitrogen until laboratory analysis.

2.2. Pigment Concentration. Pigments were extracted in 100% acetone for 24 h with trans-beta-apo-carotene as internal standard in a freezer at −20°C, with a previous three-minute sonication. Pigment extract was filtered with 0.2 μm acrodisc filters and injected into a Varian HPLC system with a degasser and *Adsorbosphere* C8 column (150 × 4.6 mm, 3.5 μm particle size). A two-solvent gradient, methanol and ammonium acetate (70 : 30 v : v), was used following the methodology described by Barlow et al. [17]. The HPLC pigment standards were purchased from Sigma-Aldrich and DHI. They were quantified with a spectrophotometer using published extinction coefficients [18] and used to identify pigment peaks and calibrate pigment concentrations based on the peak areas.

Pigment information was used to calculate phytoplankton size fractions (micro, nano, and picoplankton) according to Uitz et al. [19].

2.3. Particulate Absorption Coefficient. In the laboratory, filters were saturated with filtered seawater, which had been irradiated with UV lamps (25 W) and the optical density (OD) was measured on a Perkin-Elmer Lambda 10 spectrophotometer with integrating sphere, following the procedure in Mitchell et al. [20]. OD was measured from 400 to 750 nm with a resolution of 1 nm before and after rinsing the filters with hot methanol [20] for 15 min twice. Absorption coefficients for a particles and not pigmented particles, that is, $a_p(\lambda)$ and $a_d(\lambda)$, were determined using the equation:

$$a(\lambda) = \left(\frac{2.303S}{V}\right)\left(0.4068\mathrm{OD} + 0.368\mathrm{OD}^2\right), \quad (1)$$

where S is the filter clearance area, V is the filtered volume, and 0.4068 and 0.368 are the coefficients to correct the increase in path length caused by multiple scattering in the glass-fiber filter, which were previously determined for this spectrophotometer.

Phytoplankton absorption $a_{ph}(\lambda)$ was determined by the difference between absorption by total particulate matter, $a_p(\lambda)$, and absorption by nonpigmented material, $a_d(\lambda)$. The specific absorption coefficient by phytoplankton ($a^*_{ph}(\lambda)$), with units $\mathrm{m}^2\ (\mathrm{mg\ Chl}a)^{-1}$, was obtained by dividing $a_{ph}(\lambda)$ (m^{-1}) by Chl*a* ($\mathrm{mg\,m}^{-3}$) measured by HPLC. To compare curve shapes, normalized absorption (A, dimensionless) was plotted, which was calculated by normalizing the spectrum $a_{ph}(\lambda)$ to the absorption maxima in the blue (around 440 nm).

2.4. Satellite Images. Sea-viewing Wide Field-of-View Sensor (SeaWiFS) and Moderate resolution Imaging Spectroradiometer (MODIS/Aqua) images were processed at 1 km spatial resolution for the entire study period using SeaDAS V5.5 to obtain $\mathrm{Chl}a_{\mathrm{SAT}}$. For comparison between the *in situ* data and satellite products and to minimize georeference errors, median values were computed for all products in a 3-by-3 pixel window centered on the locations of the oceanographic stations. Furthermore, the coefficient of variation (CV) was computed for the Chl*a* within each 3-by-3 window, and

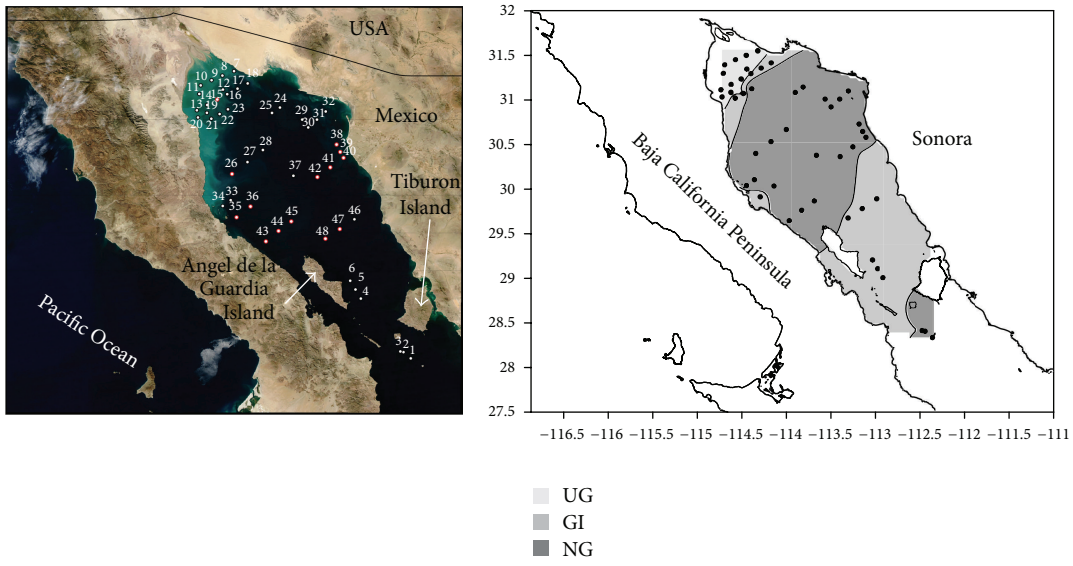

Figure 1: (a) Location of the oceanographic stations where measurements and sample collection were taken during cruise. Symbols marked with a red circle are stations where radiometric (SIMBADA) measurements were taken. (b) Bio-optical regions defined according to the first optical depth. The area colored with light gray is the Upper Gulf region (UG), medium gray background is the Great Island region (GI), and the dark gray background indicates the Northern Gulf region (NG).

the retrieved value was excluded if CV > 0.2. This process was carried out to avoid strong variation from nonhomogeneous regions within each window. For the temporal threshold coincidence between the satellite and *in situ* measurements, a ±3 hour window around the satellite overpass was considered, which follows the NASA criterion [21].

The calculation of Chla_{SAT} from SeaWiFS data is based on OC4V4 algorithm while from MODIS data it is based on OC3 algorithm [22], and Chla_{SAT} was evaluated against *in situ* Chl*a*. In the comparisons, SeaWiFS and *in situ* Chl*a* ($N = 26$), MODIS and *in situ* Chl*a* ($N = 22$), and the average Chl*a* from SeaWiFS and MODIS and *in situ* Chl*a* ($N = 28$) were used.

The OC4V4 algorithm was applied to SIMBADA data considering that SIMBADA has a band centered at 560 nm while SeaWiFS is 555 nm; that is, the effects of different SeaWiFS and SIMBADA spectral bands were ignored. These effects are expected to be much smaller than algorithm performance.

3. Results

3.1. Bio-Optical Regions. The 1OD was used as an index to define patterns in the optical properties of waters from the study area. Three regions were identified (Figure 1(b)) and named according to their geographical location. The UG region (1OD < 3 m) included stations located in the shallow Upper Gulf. The Northern Gulf region or NG (1OD > 5 m) included stations mostly located in the central part of the study area, although there were three stations in the southernmost zone. Finally, the GI region (3 m < 1OD < 5 m) had stations located in the Great Isles zone. Five stations to the north and between the UG and NG regions could be classified as belonging to the GI region considering its 1OD values, but we decided to consider this area as a transitional zone between the UG and NG. The selection of the optical depths (3 and 5 m) was based on a cluster and a stepwise discriminant analysis. The cluster analysis divided stations into groups and the second was used to confirm which station belongs to each group.

3.2. In Situ Chla and Pigments. *In situ* Chl*a* shows a strong spatial variability with values from 0.53 to 3.28 mg/m^3 (Figure 2(a)), with the lowest values on station 36 in the NG and the highest ones on station 22 in the UG region. Most stations were dominated by microplankton size fraction (Figure 2(b)), with exception of station 27 where picoplankton contributed by more than 80% to Chl*a*.

Some phytoplankton pigments can be used as markers of certain microalgae groups [17]. We used pigment composition to evaluate phytoplankton community composition according to Table 1, modified from Jeffrey et al. [18].

The UG region presented the highest concentration of the pigment Fucoxanthin, indicating the presence of diatoms, followed by Chlorophyll *b*, Hexanoyloxyfucoxanthin, Zeaxanthin, and Alloxanthin. The high ratio of Fucoxanthin/Chl*a* coincides with Chl*a* higher than 1.5 mg/m^3 and the highest Chl*a* of the entire area was observed on station 22 (Figure 2(a)), where this ratio was almost one. Santamaria-del-Angel et al. [23] mentioned that diatoms are the dominant phytoplankton group in this region, and also that Chl*a*/cell is higher due to their acclimation to the high turbidity characteristic of this zone.

The transition zone corresponds to stations 16, 17, 18, 20, and 21 (Figure 2). From these we only obtained pigment data

Table 1: Phytoplankton pigments detected in the study samples useful as diagnostic markers (adapted from Jeffrey et al., 1997 [18]).

Pigment	Abbreviation	Algal groups
Monovinyl chlorophyll *a*	Chl*a*	All groups except *Prochlorophytes*
Chlorophyll *b*	Chl*b*	Chlorophytes, Prasinophytes, euglenophytes
19′-Butanoyloxyfucoxanthin	But	Chrysophytes, prymnesiophytes
Fucoxanthin	Fuco	Diatoms, prymnesiophyte, chrysophytes, Raphidophytes
19′-Hexanoyloxyfucoxanthin	Hex	Prymnesiophytes
Peridinin	Peri	Dinoflagellates
Neoxanthin	Neo	Chlorophytes, Prasinophytes
Alloxanthin	Allo	Cryptophytes
Zeaxanthin	Zea	Cyanobacteria (including *Prochlorococcus*), Rhodophytes, Prochlorophytes, Chlorophytes, Estigmatophytes

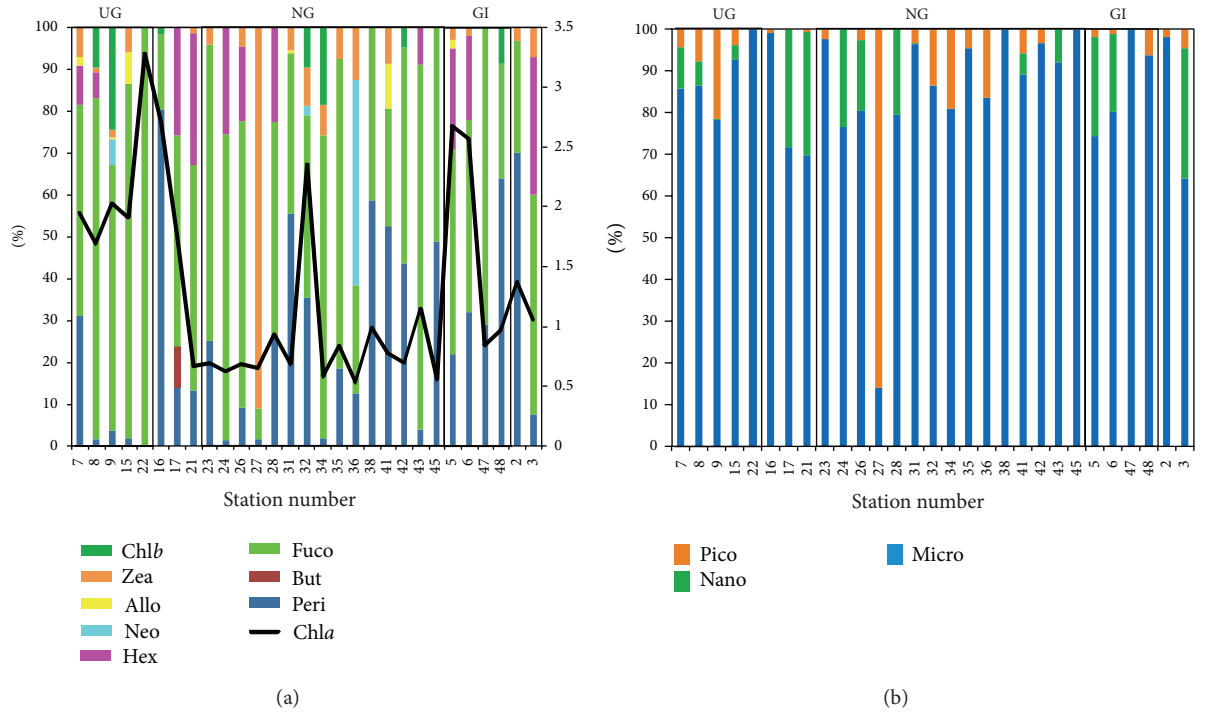

Figure 2: (a) The ratio pigment : Chl*a*, expressed in percent, is indicated in vertical bars (left axis). The bar color corresponds to some specific pigment as indicated in the legend. Pigment abbreviation is indicated in Table 1. The black continuous line is Chl*a* concentration (mg/m^3, right axis); (b) percentage contribution of phytoplankton size fractions microplankton, nanoplankton, and picoplankton to Chl*a*. Black boxes separate those stations classified inside each bio-optical region (UG: Upper Gulf; NG: Northern Gulf; GI: Great Islands region).

on stations 16, 17, and 21. The ratio Peridinin : Chl*a* increased in comparison with the level in the UG region and it was up to 0.8 in station 16. At the other two stations the contribution of Peridinin was up to 0.16 while Hexanoyloxyfucoxanthin was increased by up to 0.3, while Chl*a* was decreased to 0.8 mg/m^3.

The NG regions were characterized by Chl*a* lower than 1 mg/m^3, except station 32 located close to the east coast of the Gulf. In addition, there is a general increase of Zeaxanthin, Hexanoyloxyfucoxanthin, and Peridinin. At station 27 Zeaxanthin/Chl*a* ratio was almost 0.9, while at station 36 Neoxanthin/Chl*a* was high (~0.5).

In region GI Chl*a* is higher although values are lower than in region UG, and Zeaxanthin is barely observed. Hexanoyloxyfucoxanthin is found in increased proportion, while the Peridinin ratio is up to 0.7 at station 48 (Figure 2).

3.3. Light Absorption Coefficient. The phytoplankton absorption coefficient $a_{ph}(440)$ varied between 0.023 and 0.187 m^{-1}, the lowest at station 43 located in the NG and the highest at station 6 (GI region) (Figures 3(b), 3(d), and 3(f)). The coefficient $a_{ph}(675)$ varied between 0.007 and 0.1 m^{-1}, with minimum and maximum at the same stations above. There is

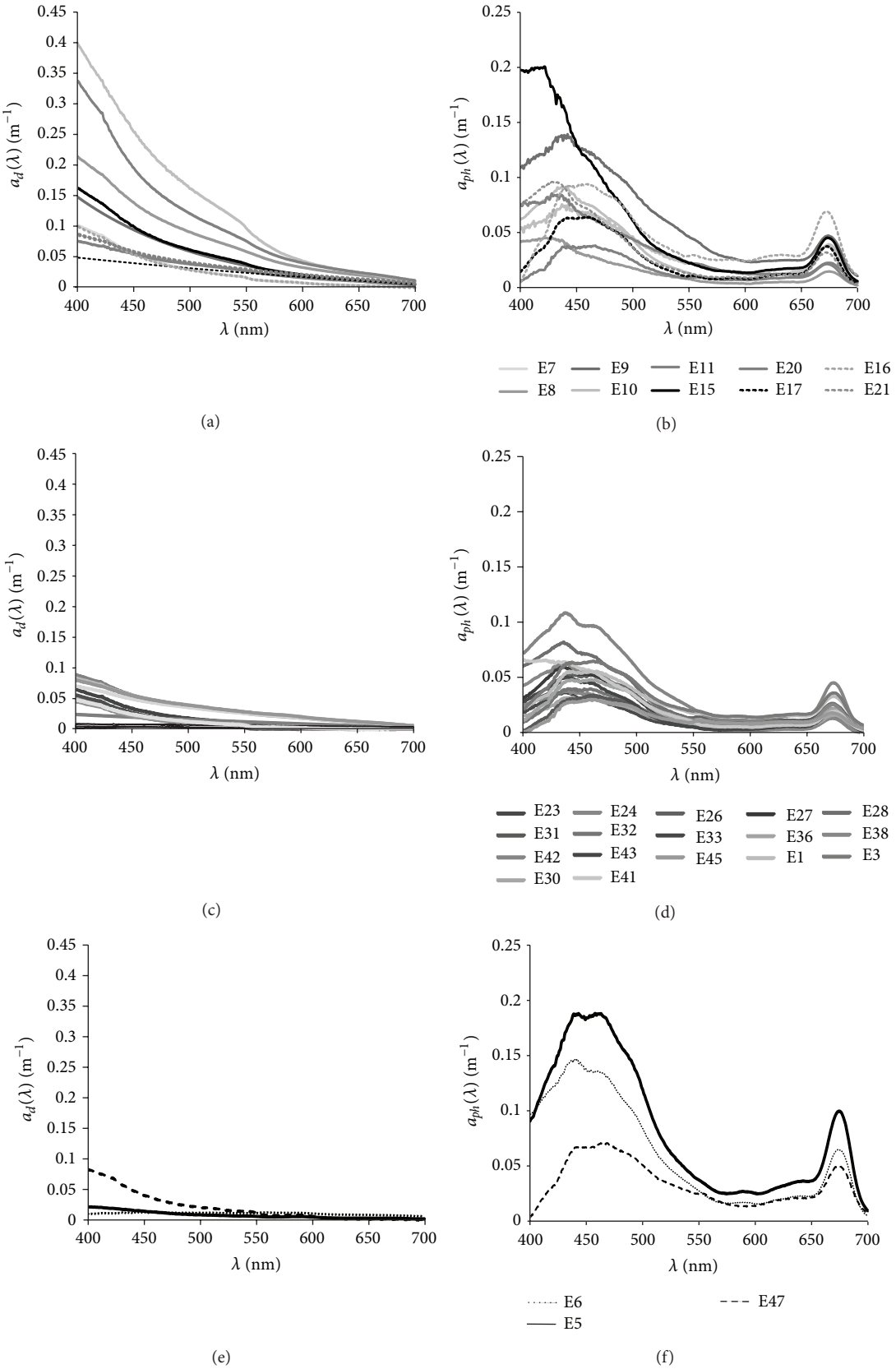

FIGURE 3: Nonpigmented particles absorption coefficient $a_d(\lambda)$ (m^{-1}) (a, c, e) and phytoplankton absorption coefficient $a_{ph}(\lambda)$ (b, d, f) grouped by bio-optical region. (a) and (b) Upper Gulf, (c) and (d) Northern Gulf, and (e) and (f) Great Isles. Dashed lines indicate those stations in the transition zone.

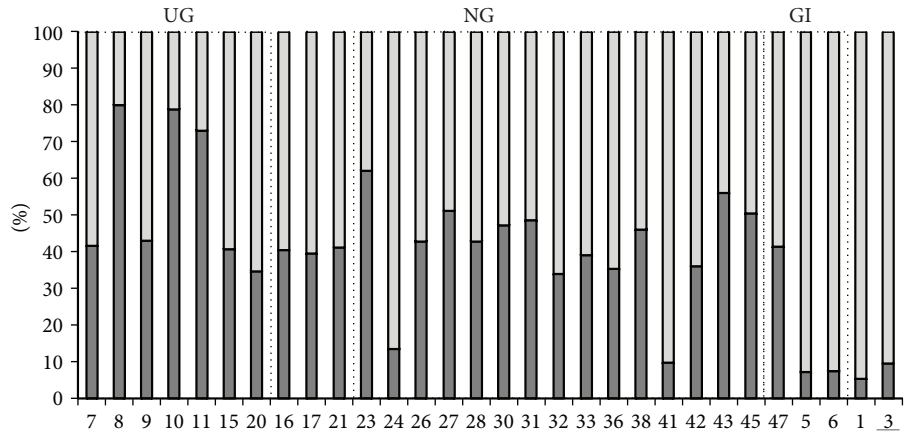

Figure 4: Percentage contribution of phytoplankton (light gray) and nonpigmented material (dark gray) to light absorption. Vertical dotted lines group stations inside each bio-optical region (UG: Upper Gulf; NG: Northern Gulf; GI: Great Isles region).

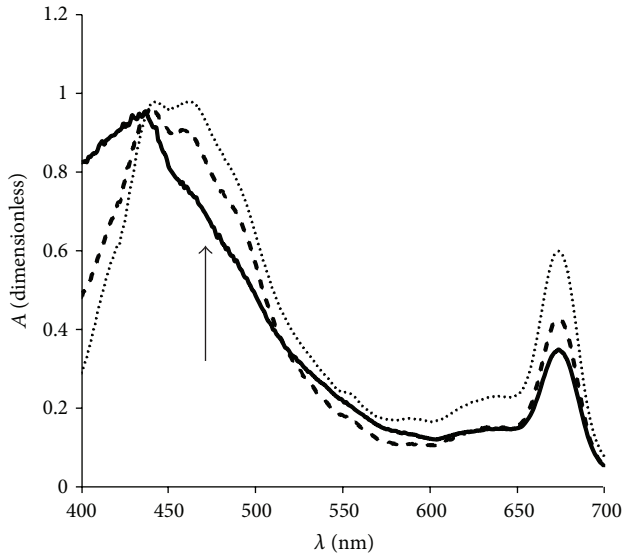

Figure 5: Average normalized absorption spectra of phytoplankton for each bio-optical region; the arrow indicates the wavelength with stronger differences among regions. UG (continuous line), NG (dotted line), and GI (dashed line).

a strong spatial variability in magnitude, with a tendency to lower values in the NG region.

The absorption coefficient by nonpigmented material at 440 nm [$a_d(440)$] varied between 0.003 and 0.28 m^{-1}, with values decreasing from north to south (Figures 3(a), 3(c), and 3(e)). The individual contribution of nonpigmented material and phytoplankton for light absorption was also analyzed (Figure 4) and a gradual decrease of $a_d(440)$ contribution from the UG to the GI with average values of 56% in the UG region, 41% in the NG region, and 18% in the GI region was observed.

The shape of the absorption spectra (Figure 5) has the two Chl*a* absorption maxima around 440 and 675 nm and an additional broad maximum at wavelengths between 450 and 500 nm, which is the highest in the NG region and slightly lower in the GI region.

The absorption coefficients $a_{ph}(440)$ and $a_{ph}(675)$ were compared to Chl*a* and a linear fitting between log-transformed data provided a low R^2 of 0.24 for $a_{ph}(440)$ ($N = 30$) and 0.33 for $a_{ph}(675)$. When compared with the fit proposed by Bricaud et al. [24] (data not shown), a lot of dispersion is observed, especially at 440 nm. The chlorophyll-specific phytoplankton absorption at 440 nm [$a^*_{ph}(440)$] decreased with Chl*a* and ranged from 0.017 to 0.155 m^2 mg Chla^{-1}, while the chlorophyll-specific phytoplankton absorption at 675 nm [$a^*_{ph}(675)$] also decreased varying from 0.006 to 0.065 m^2 mg Chla^{-1}. The general tendency is a decrease with the Chl*a* increase, as expected, although with a high dispersion as observed above for $a_{ph}(440)$ and $a_{ph}(675)$ (Figure 6).

Light absorption by nonpigmented material [$a_d(440)$] did not covary with Chl*a* (Figure 7(a)) with the exception of the UG where an inverse relationship was observed. This indicates that in this region stations with high Chl*a* had generally less inorganic particles. A regression line was adjusted to these data and the resulting equation (R^2 = 86%, 95% confidence) was

$$a_d\,(440) = 0.377 - 0.142\text{Chl}a. \tag{2}$$

The attenuation coefficient K_d was also compared to Chl*a* (Figure 7(b)) and an inverse relationship was also observed for UG data, while a positive but weak one was observed for the other sites. A regression line was adjusted for those UG data and the resulting equation (R^2 = 65%, 95% confidence) was

$$K_d = 1.93 - 0.573\text{Chl}a. \tag{3}$$

3.4. Variability of Reflectance Spectra. The reflectance spectra variability is indicated in Figure 8. Unfortunately, in the UG region we only have data for station 15, which has the highest $R(\lambda)$, especially at 560 nm, that can be related to high concentrations of total suspended matter. The NG region was

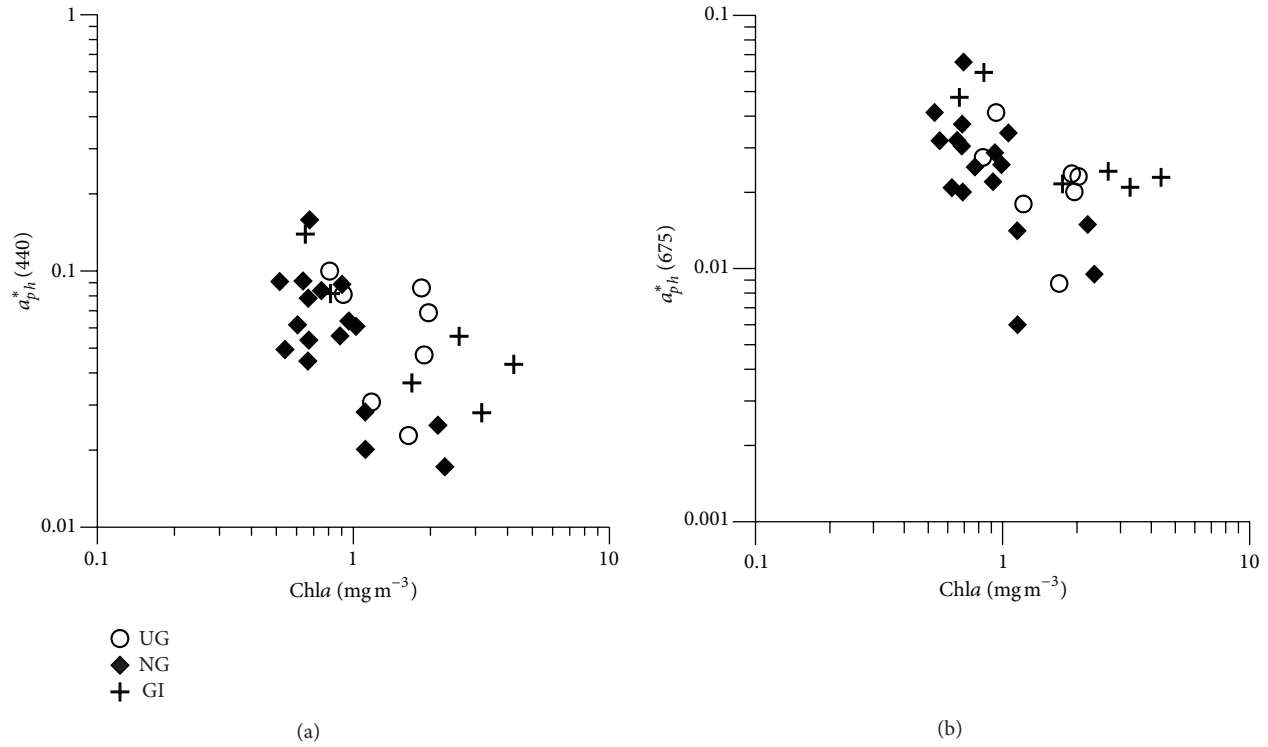

FIGURE 6: Variations of the specific absorption coefficient of phytoplankton at 440 nm (a) and 675 nm (b) (m^{-2} mg Chl*a*) as a function of Chl*a* (mg m^{-3}).

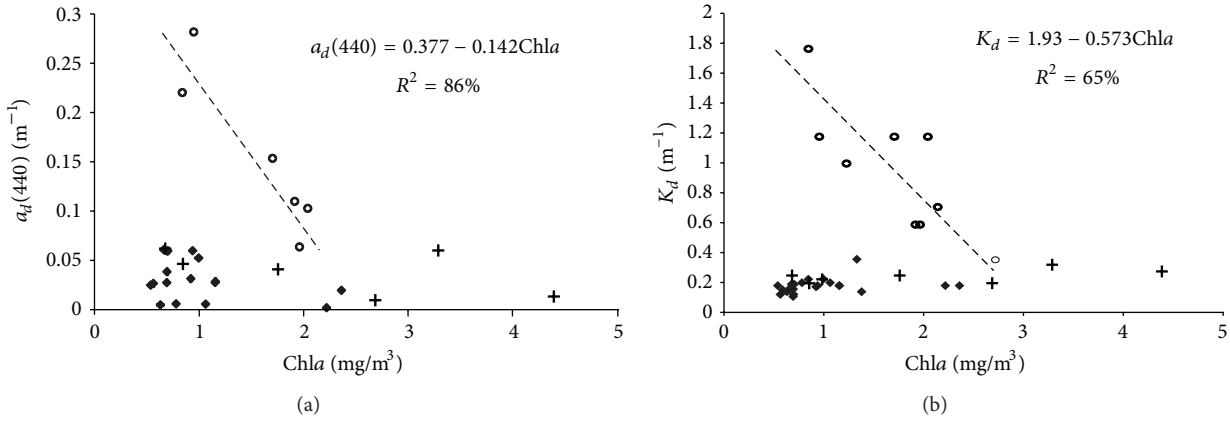

FIGURE 7: (a) Variation of $a_d(440)$ (m^{-1}) as a function of Chl*a*. (b) Variation K_d (m^{-1}) as a function of Chl*a*. Open circles are Upper Gulf stations, black diamonds are Northern Gulf stations, and crosses are Great Isles stations. Regression for the UG data is shown as a dashed line and the fitted equation and the coefficient of determination (R^2) are also shown.

the one with the highest number of data, 12 stations, while there were only data at two stations for region GI (stations 47 and 48). Due to variability in water composition, no distinct difference is apparent between the reflectance spectra of the NG and GI regions, which therefore can hardly be classified based on marine reflectance.

3.5. Chla_{SAT} and Bio-Optical Algorithm Evaluation. Chla_{SAT} images during the study period demonstrated a strong variability in the study area (Figure 9) with the appreciation of several structures like eddies, filaments, and meanders. In general Chla_{SAT} is higher to the north related to the UG zone, to the south around the Great Isles region (GI), and along the west side of the NG. However, a decrease of Chla_{SAT} is noted in this last zone, especially after June 9.

The performance of the empirical algorithms OC4V4 and OC3 was evaluated through the comparison of Chla_{SAT} with *in situ* Chl*a* (Figures 10(a) and 10(b)). For SeaWiFS Chla_{SAT} (Figure 10(a)), the calculated RMSE was 36% while the BIAS was 28% ($N = 26$). For MODIS Chla_{SAT} (Figure 10(b)),

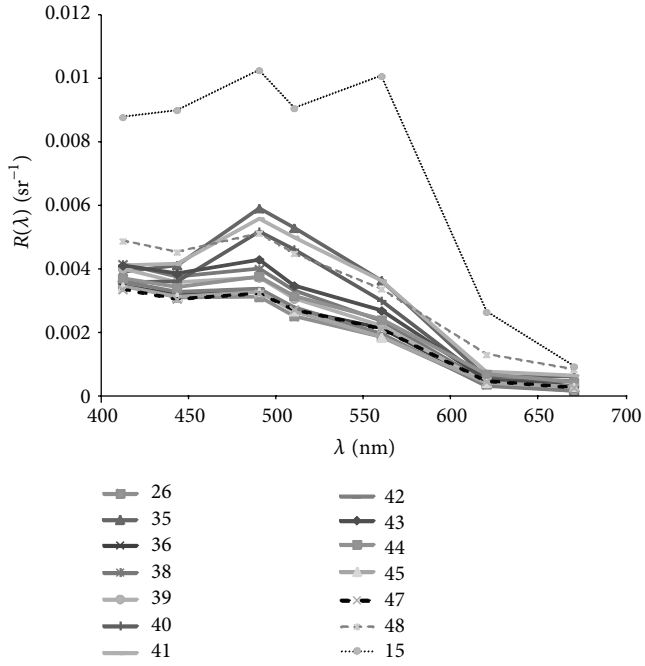

FIGURE 8: Reflectance spectra, $R(\lambda)$ in sr^{-1}, for each station. Continuous lines are for NG stations and dashed lines for GI stations.

RMSE and BIAS were similar, that is, 29% and a 22% (N = 22), respectively. Finally, we calculated the average between MODIS and SeaWiFS Chl*a* and these data were compared to *in situ* Chl*a*, which resulted in a RMSE of 33% and a BIAS of 26% (N = 28).

The satellite and *in situ* maximum reflectance ratios (MRRs) were also compared (Figure 10(c)). They were calculated using the highest reflectance value in the blue ($R(443)$, $R(490)$, or $R(510)$) divided by $R(555)$ or $R(560)$. Results show that satellite values are lower than the SIMBADA values, explaining the higher (overestimated) satellite estimates of Chl*a* (Figures 10(a) and 10(b)). The lower satellite values are due to lower reflectance in the blue.

3.6. Statistical Analysis. The differences among the proposed bio-optical regions were firstly examined through the comparison of $a_d(\lambda)$, $a_{ph}(\lambda)$, and the shape A, using a nonparametric Kruskall-Wallis test for independent samples. Results indicated that regions UG, NG and GI are statistically different (95% confidence level) from each other. However, when comparing the reflectance spectra using the same test the NG and GI regions were not significantly different, although both are different from the UG. This was mentioned qualitatively in Section 3.4. The differences among regions are summarized in Table 2.

4. Discussion

4.1. Bio-Optical Regions. In situ Chl*a* indicates the strong spatial variability of the study area, which agrees with the proposed bio-optical classification, that is the highest values in the UG, a decrease in the NG, and a new increase in the GI (Figure 2). The difference between the UG and NG is especially remarkable, as previously noted by other studies based on some hydrographic and biological aspects [10, 11]. These changes in Chl*a* are also linked to changes in phytoplankton community structure (size and composition) which could be inferred from pigment composition [19, 25].

In this study, the dominance of microplankton could be observed in the entire study area, with a slight increase in the proportion of picoplankton in the NG region (Figure 2(b)), which is characteristic of zones with more oligotrophic waters [24, 26]. The index used to estimate size fraction [19] considers Fucoxanthin and Peridinin to infer the proportion of microplankton, which indicates the presence of diatoms and/or dinoflagellates, respectively (Table 1). These pigments were dominant in our data (Figure 2(a)) but there was observed a higher proportion of Fucoxanthin in the UG while in the NG and GI region Peridinin increased its proportion. It is also important to observe the increase in the pigment Zeaxanthin in the NG, which attains its maximum value at station 27, which results in the dominance of picoplankton in this station (Figure 2(b)). In a natural environment, shifts in the hydrological features of the water column are related to changes in nutrient concentration, which in turn is associated with the modification of phytoplankton composition and their mean size [19]. As previously mentioned, diatoms are the dominant group in the UG region [23] and a high biomass of this group has been also reported in the GI region [27, 28] and confirmed in our data.

Larger cells suffer with a higher package effect and lower specific absorption coefficients [24]. It is assumed that higher Chl*a* are related to larger cells [24] and as a consequence an inverse relationship between Chl*a* and the specific absorption coefficients $a^*_{ph}(440)$ and $a^*_{ph}(675)$ is expected [26]. In our data Chl*a* varied between 0.53 and 3.28 mg/m^3 (Figure 2(a)) but there was almost no change in size fraction (Figure 2(b)) which can explain the high dispersion in the observed relationship (Figure 6). This dispersion was especially high for the UG data and at 440 nm. Millán-Núñez et al. [27] also observed more variability at 440 nm than at 675 nm when comparing $a^*_{ph}(\lambda)$ with Chl*a* for some stations in our study area. They attributed this pattern to chlorophyll per cell volume which was not independent of cell size, as assumed in models that explain the inverse relationship between $a^*_{ph}(\lambda)$ and cell size [24]. In addition, the inverse relationship between these parameters may not necessarily hold in coastal waters because of events such as upwelling, advection, fronts, and freshwater inputs, as well as the complexity of light field conditions [29, 30], processes that are frequent in our study area. In particular the UG is a region with very complex hydrodynamics, high concentrations of suspended matter, and consequently very peculiar light conditions [11, 23] in comparison with the southernmost regions. The concentration of suspended matter inferred from $a_d(440)$ had the highest contribution to light absorption in the UG, while it had the lowest contribution in the GI region (Figure 4). Taking into account the observed differences among the three bio-optical regions, we evaluated the relationship between

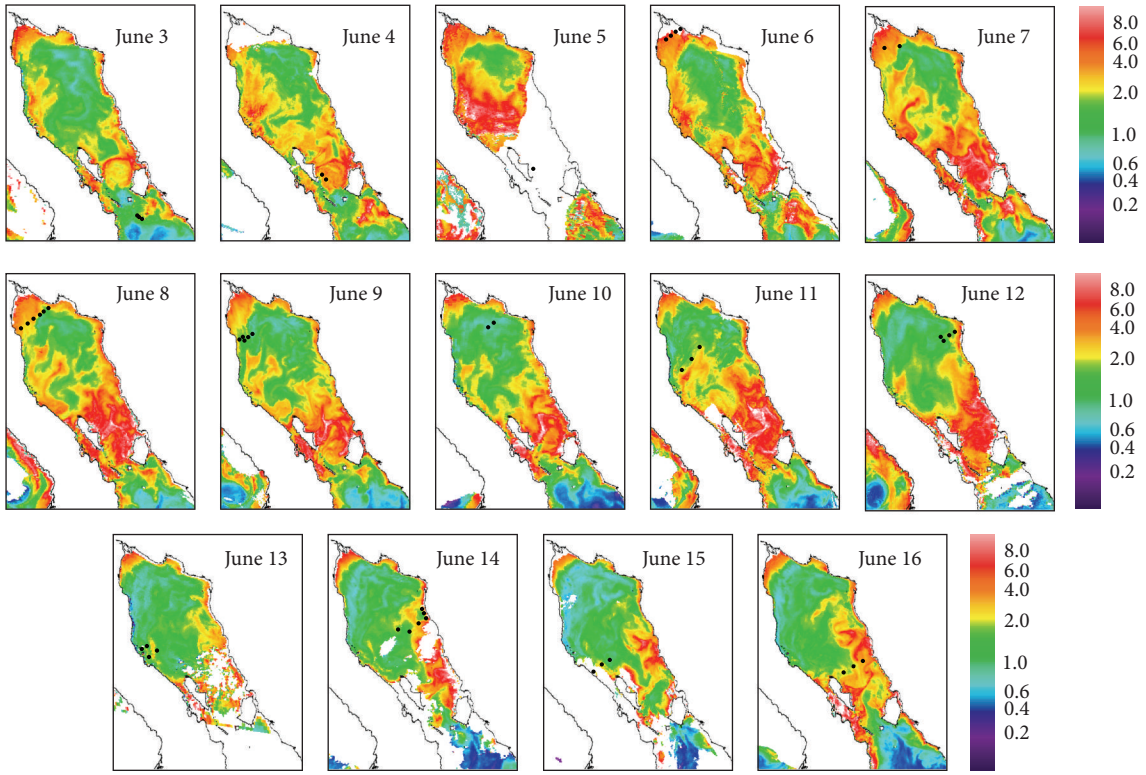

FIGURE 9: LAC SeaWiFS Chl*a* images (mg/m^3). Station position for each sampling date is indicated with black circles.

$a^*_{ph}(440)$ and Chl*a* for each one individually given that for the UG a power low fit resulted in a R^2 of 9%, while for the NG it was 53% ($a^*_{ph}(440) = 0.0472\text{Chl}a^{-1.006}$) and for the GI it was 68% ($a^*_{ph}(440) = 0.0795\text{Chl}a^{-0.631}$). This pattern is an indication of the shift in bio-optical conditions from north to south going from turbid and eutrophic to mesotrophic waters. In addition, different associations were observed between variables in the UG; an inverse relationship between $a_d(440)$ and Chl*a*, and between K_d and Chl*a* (Figure 7). An inverse relationship between $a_d(440)$ and Chl*a* is an indication that Chl*a* increases when nonpigmented particles are found in low concentration, that is, in clearer waters. Besides, the tendency observed for K_d can be explained by the high concentration of nonalgal and mineral particles in the UG (Figures 3 and 4).

Phytoplankton absorption spectra also show important differences among regions with a tendency to lower values in the NG (Figure 3(d)) and at most stations of the UG (Figure 3(b)). In this region, only stations 9 and 15 presented values higher than 0.1 m^{-1}. In the GI region (Figure 3(f)), only station 47, located to the north and in the limit with the NG, presented values lower than 0.1 m^{-1}. At this station the proportion of microplankton was the highest (Figure 2(b)), while at stations 5 and 6 the proportion of nanoplankton increased. When we analyzed the average shape of the absorption spectra (Figure 5), the differences among regions were more evident, and the absorption increase around 480 nm from the UG to the NG and a new decrease in the GI region are remarkable. Indeed, the significance of these differences (magnitude and shape) was statistically tested and confirmed. An absorption increase at wavelengths between 440 and 550 nm indicates a higher proportion of carotenoids: Chl*a* or photoprotective pigments [19, 23, 30]. A low concentration of photoprotective pigments can be inferred in the UG region as an indication of low-light conditions associated with the high turbidity.

The reflectance spectra showed a small variability in the study area (Figure 8) with the exception of station 15, the only one in the UG, which has a strong signal at 560 nm related to high scattering by nonpigmented and mineral particles [30], which was confirmed by high nonpigmented particles absorption values (Figure 3(a) and Table 2). The statistical analysis confirmed the observed difference between the UG station and the others.

4.2. Chla_{SAT} and Bio-Optical Algorithm Evaluation. The large spatial and temporal variability of the study area is manifested in Chla_{SAT} (Figure 9) with gradients associated with the defined bio-optical regions. In general, Chla_{SAT} is higher to the north related to UG region, decreases in the NG region, and increases in the GI region. However, it has to be noted that Chla_{SAT} decreased in this last zone, especially after June 13 when the extension of the central oligotrophic region increased. In fact, a frontal zone is clearly visible in the images (Figure 9), as also noted by Sánchez-Velasco et al. [11], in which are located those stations classified as in

Table 2: Average (minimum and maximum in parenthesis) values for each bio-optical region of first optical depth (1OD), chlorophyll-*a* concentration (Chl*a*), phytoplankton light absorption coefficient at 440 nm ($a_{ph}(440)$) and 675 nm ($a_{ph}(675)$), nonpigmented particles light absorption coefficient at 440 nm ($a_{ph}(440)$), percent contribution of nonpigmented particles to light absorption (%d), reflectance at 560 nm ($R(560)$), and maximum reflectance ratio (MRR). In column "Region" number in parenthesis is the number of data used for average calculations for all data except $R(560)$ and MRR. For these last two variables the number of data used for calculation is indicated at the right of the slash.

Region	1OD (m)	Chl*a* (mg m^{-3})	$a_{ph}(440)$ (m^{-1})	$a_{ph}(675)$ (m^{-1})	$a_d(440)$ (m^{-1})	%d	$R(560)$ (sr^{-1})	MRR
UG (7/1)	1.34 (0.56–2.82)	1.51 (0.83–2.03)	0.089 (0.037–0.161)	0.033 (0.015–0.047)	0.156 (0.065–0.282)	56	0.01	1.018
NG (17/8)	4.19 (3.11–5.00)	0.98 (0.53–2.35)	0.051 (0.023–0.108)	0.023 (0.007–0.045)	0.032 (0.003–0.062)	41	0.0025 (0.0018–0.0036)	1.653 (1.541–1.774)
GI (3/2)	6.15 (5.08–9.6)	2.63 (0.84–4.38)	0.134 (0.067–0.187)	0.072 (0.05–0.1)	0.025 (0.011–0.048)	18	0.0027 (0.0021–0.0034)	1.523 (1.522–1.526)

a transitional zone (stations 16, 17, and 21) that were sampled in June 8 and 9. After these two days the frontal zone moved farther north and Chla_{SAT} in the central zone (NG) of the study area gradually decreased until the end of the sampling period and in coincidence with the *in situ* sampling. It has to be noted that the west coast off Baja California peninsula presented higher Chla_{SAT} with filaments that penetrate into the central part of the gulf. This zone was classified as NG despite the differences in Chla_{SAT} from coast to coast and it was probably because stations that defined this region were sampled when this area had the lower Chla_{SAT} and those high concentrations from the west coast strongly decreased (June 11 to 16). When a synoptic map is created joining the information from all stations sampled during a cruise, it has to be considered that during the cruise oceanographic conditions are changing. As previously noted, the study area is strongly affected by tidal mixing, especially around the sills of the midriff archipelago region (GI) and in the shallow UG and by a complex circulation pattern that is visible in Chla_{SAT}.

The satellite data product accuracy generally obtained by the international missions is ±35% for Chl*a* in open ocean waters [31], which is compatible with performance statistics reported in this work (Figures 10(a) and 10(b)), although with differences between sensors. However, a positive BIAS was observed for both sensors (SeaWiFS and MODIS), indicating an overestimation of *in situ* Chl*a*. This is to be expected if we consider that the region is clearly influenced by high concentrations of nonpigmented material, especially to the north (UG and some stations of the NG) (Figure 4 and Table 2). The relatively good performance of the algorithms can be explained by some compensation among variables responsible for $R(\lambda)$ variability; that is the backscattering coefficient ($b_b(\lambda)$) can be higher in the green but it will be also high in the blue, but explaining how does this compensation occurs is difficult because we do not have measurements of $b_b(\lambda)$ or even of CDOM absorption coefficient. In addition, the satellite $R(\lambda)$ estimates in the blue are usually too low, resulting in too low satellite MRR (Figure 10); therefore satellite Chl*a* is too high. This may be due not only to absorption by nonalgal material, in particular sediments, and CDOM, but also to the influence of desert and continental aerosols (i.e., absorbing aerosols) over the Gulf region.

5. Conclusion

Our results indicate that the Northern Gulf of California can be classified into three bio-optical regions associated to previously identified surface circulation patterns and bottom topography. Besides, a transition zone was identified to the north, and the three southernmost stations (1, 2, and 3) are probably part of another region with different characteristics compared with the hither GI region. Pegau et al. [13] examined some inherent optical properties of these waters, focusing mainly on the south of our study area (Guaymas Basin) although sampling some stations also in the GI and NG regions. They considered the NG as belonging to Case 2 waters while those to the south belong to Case 1 (including the GI region). In our study, the differences between the NG and GI regions were considered significant when comparing the absorption spectra but they were not when comparing the reflectance spectra. Marine reflectance varies as a function of the ratio of the backscattering coefficient $b_b(\lambda)$ and the absorption coefficient $a(\lambda)$ [32], and we have measured only the last one. In addition, the absorption coefficient $a(\lambda)$ is a result of the combined contribution of water components like phytoplankton, nonpigmented particles, and colored dissolved organic matter ($a_{CDOM}(\lambda)$), of which we did not measure the last one, even though it was previously considered as important in the study area [13]. Thus our observations appear to confirm the differences in both $b_b(\lambda)$ and $a_{CDOM}(\lambda)$ between the NG and GI explain the similarities between $R(\lambda)$ in these two regions. In addition, *in situ* absorption data were from surface samples while $R(\lambda)$ comes from the first optical depth, which ranged from 3 to 5 m at the GI region and it was higher than 5 m at the NG. Furthermore, the proportion of $a_d(440)$ to light absorption (Figure 4 and Table 2) in the GI region was significantly lower than in the NG, although being very similar to the proportion at those stations to the south. It means that our observations probably confirm those of Pegau et al. [13]; that is, the NG region (and surely the UG) belongs to Case 2 while those to the south to Case 1. However, even when the UG and NG waters are considered as Case 2 they do have different bio-optical characteristics. This implies that classifying this area as Case 1 or Case 2 is incomplete and instead both biological

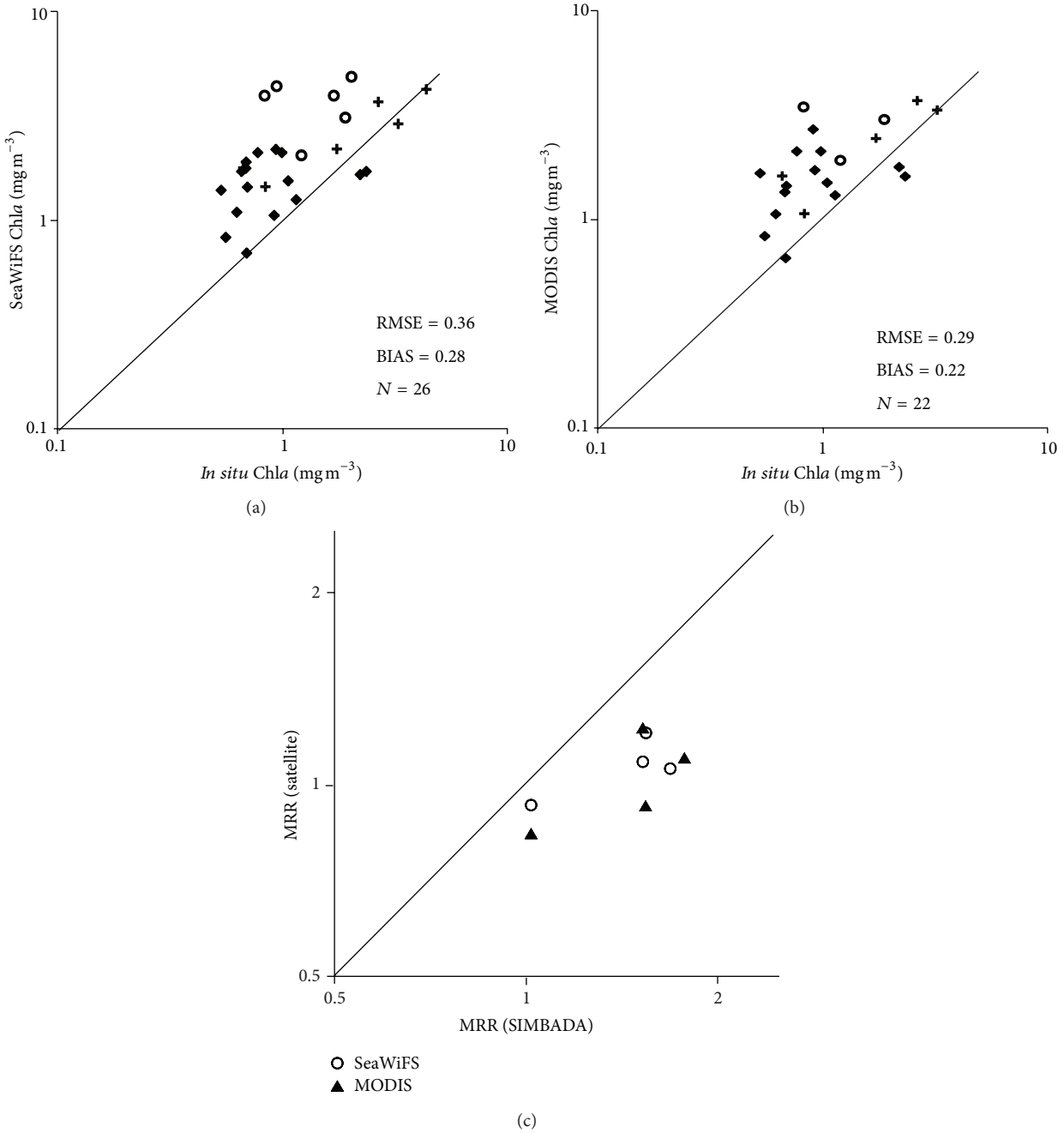

Figure 10: (a) Comparison between *in situ* Chl*a* and SeaWiFS Chl*a* (mg m^{-3}) (N = 26) and (b) between *in situ* Chl*a* and MODIS Chl*a* (N = 22), with the indication of RMSE and BIAS statistics; the 1:1 line is indicated for reference. Open circles are Upper Gulf stations, black diamonds are Northern Gulf stations, and crosses are Great Islands stations. (c) Comparison between satellite and *in situ* (SIMBADA) maximum reflectance ratio (MRR).

and optical properties should be considered to gain a better understanding of the $R(\lambda)$ variability in the Gulf region and the underlying biogeochemical processes.

The bio-optical spatial variability of the study area has important implications for interpreting variations in ocean color. Although reasonable agreement were found between measured and satellite-estimated Chl*a*, regional refinements of the empirical algorithm that take into account differences between bio-optical regions should improve the satellite estimates of Chl*a* and also of the inherent optical properties for the study area. It should be noted that our findings are based on both (1) two weeks of observations and limited parameters and (2) one season; therefore it cannot provide a complete picture of bio-optical spatial and seasonal variability. Complementary field experiments and further research, including new cruises, are underway to understand

the bio-optical complexities of the Gulf region and develop appropriate models for the remote detection of its water composition and inherent optical properties.

Conflict of Interests

The authors declare that there is no conflict of interests regarding the publication of this paper.

Acknowledgments

This work was supported by two projects: "Ecological Monitoring of the Upper Gulf of California" financed by the David and Lucile Packard Foundation (contract no. 2009-34967) through the University of Arizona PANGAS project and "A Time Series of Marine Bio-Optical Properties off Baja California for Satellite Ocean Colour Evaluation" financed by 2008 UC MEXUS-CONACYT Collaborative Research Grants. M. Bastidas-Salamanca was supported by the UC MEXUS-CONACYT grant. R. Frouin was supported by various grants from the National Aeronautics and Space Administration.

References

[1] IOCCG, "Remote sensing of ocean colour in coastal, and other optically-complex waters," Reports of the International Ocean Colour Coordinating Group no. 3, IOCCG, Dartmouth, Canada, Edited by S. Sathyendranath, 2000.

[2] M. F. Lavín and S. G. Marinone, "An overview of the physical oceanography of the Gulf of California," in *Nonlinear Processes in Geophysical Fluid Dynamics*, O. U. Velasco-Fuentes, J. Sheinbaum, and J. Ochoa, Eds., pp. 173–204, Kluwer Academic, Dordrecht, The Netherlands, 2003.

[3] S. E. Lluch-Cota, E. A. Aragón-Noriega, F. Arreguín-Sánchez et al., "The Gulf of California: review of ecosystem status and sustainability challenges," *Progress in Oceanography*, vol. 73, no. 1, pp. 1–26, 2007.

[4] E. Palacios-Hernández, E. Beier, M. F. Lavín, and P. Ripa, "The effect of the seasonal variation of stratification on the circulation of the Northern Gulf of California," *Journal of Physical Oceanography*, vol. 32, no. 3, pp. 705–728, 2002.

[5] L. Carrillo and E. Palacios-Hernández, "Seasonal evolution of the geostrophic circulation in the northern Gulf of California," *Estuarine, Coastal and Shelf Science*, vol. 54, no. 2, pp. 157–173, 2002.

[6] J. Lopez-Calderon, A. Martinez, A. Gonzalez-Silvera, E. Santamaria-del-Angel, and R. Millan-Nuñez, "Mesoscale eddies and wind variability in the Northern Gulf of California," *Journal of Geophysical Research C: Oceans*, vol. 113, no. 10, 2008.

[7] M. L. Argote, A. Amador, M. F. Lavin, and J. R. Hunter, "Tidal dissipation and stratification in the Gulf of California," *Journal of Geophysical Research*, vol. 100, no. 8, pp. 16103–16118, 1995.

[8] S. Álvarez-Borrego and J. R. Lara-Lara, "The physical environment and productivity of the Gulf of California," in *The Gulf and Peninsular Province of the Californias*, J. P. Dauphin and B. Simoneit, Eds., vol. 47, pp. 555–567, American Association of Petroleum Geology Memorial, 1991.

[9] M. López, J. Candela, and M. L. Argote, "Why does the Ballenas Channel have the coldest SST in th Gulf of California?" *Geophysical Research Letters*, vol. 33, no. 11, Article ID L11603, 2006.

[10] L. Sánchez-Velasco, M. F. Lavín, M. Peguero-Icaza et al., "Seasonal changes in larval fish assemblages in a semi-enclosed sea (Gulf of California)," *Continental Shelf Research*, vol. 29, no. 14, pp. 1697–1710, 2009.

[11] L. Sánchez-Velasco, M. F. Lavín, S. P. A. Jiménez-Rosenberg, J. M. Montes, and P. J. Turk-Boyer, "Larval fish habitats and hydrography in the Biosphere Reserve of the Upper Gulf of California (June 2008)," *Continental Shelf Research*, vol. 33, pp. 89–99, 2012.

[12] E. A. Inda-Díaz, L. Sánchez-Velasco, and M. F. Lavín, "Three-dimensional distribution of small pelagic fish larvae (*Sardinops sagax* and *Engraulis mordax*) in a tidal-mixing front and surrounding waters (Gulf of California)," *Journal of Plankton Research*, vol. 32, no. 9, pp. 1241–1254, 2010.

[13] W. S. Pegau, J. R. V. Zaneveld, A. H. Barnard et al., "Inherent optical properties in the Gulf of California," *Ciencias Marinas*, vol. 25, no. 4, pp. 469–485, 1999.

[14] J. T. O. Kirk, *Light and Photosynthesis in Aquatic Ecosystems*, Cambridge University Press, Cambridge, UK, 1994.

[15] P.-Y. Deschamps, B. Fougnie, R. Frouin, P. Lecomte, and C. Verwaerde, "SIMBAD: a field radiometer for satellite ocean-color validation," *Applied Optics*, vol. 43, no. 20, pp. 4055–4069, 2004.

[16] G. Bécu, *Contribution a la vérification des observations spatiales de la couleur de l'océan a l'aide du réseau de radiometers SIMBADA [Ph.D. thesis]*, Université des Sciences et Technologies de Lille, Villeneuve-d'Ascq, France, 2004.

[17] R. G. Barlow, D. G. Cummings, and S. W. Gibb, "Improved resolution of mono- and divinyl chlorophylls *a* and *b* and zeaxanthin and lutein in phytoplankton extracts using reverse phase C-8 HPLC," *Marine Ecology Progress Series*, vol. 161, pp. 303–307, 1997.

[18] S. W. Jeffrey, R. F. C. Mantoura, and S. W. Wright, *Phytoplankton Pigments in Oceanography: Guidelines and Modern Methods*, UNESCO Publishing, Paris, Farnce, 1997.

[19] J. Uitz, H. Claustre, A. Morel, and S. B. Hooker, "Vertical distribution of phytoplankton communities in open ocean: an assessment based on surface chlorophyll," *Journal of Geophysical Research C: Oceans*, vol. 111, no. 8, Article ID C08005, 2006.

[20] B. Mitchell, M. Kahru, J. Wieland, and M. Stramska, "Determination of spectral absorption coefficients of particles, dissolved material and phytoplankton for discrete water samples," in *Ocean Optics Protocols for Satellite Ocean Color Sensor Validation, Revision 2*, G. S. Fargion and J. L. Mueller, Eds., NASA/TM-2000-209966, pp. 125–153, 2000.

[21] S. W. Bailey, C. R. McClain, P. J. Werdell, and B. D. Schieber, "Normalized water-leaving radiance and chlorophyll a match-up analyses," NASA Tech. Memo 206892, National Aeronautics and Space Administration, Goddard Space Flight Center, Greenbelt, Md, USA, 2000.

[22] J. E. O'Reilly, S. Maritorena, B. G. Mitchell et al., "Ocean color chlorophyll algorithms for SeaWiFS," *Journal of Geophysical Research C: Oceans*, vol. 103, no. 11, pp. 24937–24953, 1998.

[23] E. Santamaria-del-Angel, R. Millán-Núñez, and G. de la Peña-Nettel, "Effect of turbidity on primary productivity at two stations in the area of the colorado river delta," *Ciencias Marinas*, vol. 22, no. 4, pp. 483–493, 1996.

[24] A. Bricaud, H. Claustre, J. Ras, and K. Oubelkheir, "Natural variability of phytoplanktonic absorption in oceanic waters: influence of the size structure of algal populations," *Journal of Geophysical Research C: Oceans*, vol. 109, no. 11, Article ID C11010, 2004.

[25] F. Vidussi, H. Claustre, B. B. Manca, A. Luchetta, and J.-C. Marty, "Phytoplankton pigment distribution in relation to upper thermocline circulation in the Eastern Mediterranean Sea during winter," *Journal of Geophysical Research C: Oceans*, vol. 106, no. 9, pp. 19939–19956, 2001.

[26] Ó. A. Barocio-León, R. Millán-Núñez, E. Santamaría-del-Ángel, A. González-Silvera, and C. C. Trees, "Spatial variability of phytoplankton absorption coefficients and pigments off Baja California during November 2002," *Journal of Oceanography*, vol. 62, no. 6, pp. 873–885, 2006.

[27] E. Millán-Núñez, J. R. Lara-Lara, and J. S. Cleveland, "Variations in specific absorption coefficients and total phytoplankton in the Gulf of California," *California Cooperative Oceanic Fisheries Investigations Reports*, vol. 39, pp. 159–168, 1998.

[28] G. Gaxiola-Castro, S. Álvarez-Borrego, S. Nájera-Martínez, and A. R. Zirino, "Internal waves effect on the Gulf of California phytoplankton," *Ciencias Marinas*, vol. 28, no. 3, pp. 297–309, 2002.

[29] A. Bricaud, M. Babin, A. Morel, and H. Claustre, "Variability in the chlorophyll-specific absorption coefficients of natural phytoplankton: analysis and parameterization," *Journal of Geophysical Research*, vol. 100, no. 7, pp. 13–332, 1995.

[30] M. Babin, D. Stramski, G. M. Ferrari et al., "Variations in the light absorption coefficients of phytoplankton, nonalgal particles, and dissolved organic matter in coastal waters around Europe," *Journal of Geophysical Research C: Oceans*, vol. 108, no. 7, 2003.

[31] C. R. McClain, "A decade of satellite ocean color observations," *Annual Review of Marine Science*, vol. 1, pp. 19–42, 2009.

[32] A. Morel and S. Maritorena, "Bio-optical properties of oceanic waters: a reappraisal," *Journal of Geophysical Research C: Oceans*, vol. 106, no. 4, pp. 7163–7180, 2001.